Visualizations of Leading Edge Cavitation in an Inducer at Different Temperatures

J.P. Franc*, E. Janson**, P. Morel***, C. Rebattet**, M. Riondet*

Laboratoire des Ecoulements Géophysiques et Industriels, BP 53, 38041 Grenoble Cedex 9, France
*** Centre de Recherches et d'Essais de Machines Hydrauliques de Grenoble, BP 95, 38402 Saint-Martin d'Hères Cedex, France*
*** Snecma Moteurs, Division Moteurs-fusées, BP802, 27208 Vernon Cedex, France*

Abstract

Visualizations of the leading edge cavity on a four-bladed inducer working with refrigerant 114 are presented. The evolution of the cavity length with the cavitation number is given for three different temperatures. These data are used to estimate the thermodynamic effect in R114. In addition, the onset of cavitation instabilities (alternate blade cavitation and rotating cavitation) are determined from the analysis of pressure fluctuations. The thermodynamic effect which affects the onset of instabilities is also estimated and compared to the one deduced from visualizations.

Nomenclature

a	thermal diffusivity of the liquid	T	temperature
c_{pl}	specific heat of the liquid	T_∞	temperature of the liquid at infinity
L	latent heat of vaporization	$\Delta T* = \dfrac{\rho_v\, L}{\rho_l\, c_{pl}}$	parameter (dimension: temperature)
p_c	pressure inside the cavity	ρ_l	density of the liquid
p_{ref}	reference pressure	ρ_v	density of the vapor
R	radius of the inducer	ω	angular velocity of the inducer

1. Introduction

This paper is devoted to an analysis of the thermodynamic effect on a typical inducer used in rocket engines turbopumps. Contrary to cold water, cryogenic liquids have specific thermodynamic properties, which make that heat transfer phenomena are not negligible. The temperature near the cavitating region is generally a few degrees below the liquid bulk temperature. This phenomenon leads to a delay in the development of cavitation and to a regular decrease of the breakdown cavitation number with increasing temperature.

A large amount of work has been done in this field. Various experiments were conducted on different geometries (venturi, ogives, hydrofoils, pumps) using diverse liquids as refrigerants and liquid cryogens (see e.g. Billet 1970, Hord 1972a, 1972b, 1973, 1974, Kovich 1970). Several theoretical approaches were also made to analyze the experimental results and predict the thermodynamic effect.

The first correlations derived by Stepanoff (1964), Moore & Ruggeri 1968 and Ruggeri & Moore 1969 were based upon the well-known B-factor, which is defined as the ratio of the vapor volume to the liquid volume involved in the vaporization process.

For a sheet cavity, Holl *et al.* (1975) and Billet *et al.* 1981 proposed to write an energy balance for the cavity based on two main parameters: (1) a flow coefficient which measures the vapor flowrate which is removed from the cavity and entrained by the liquid flow and (2) a Nusselt number which measures the convective heat transfer through the cavity interface.

Fruman *et al.* (1991) proposed to estimate the Nusselt number using an analogy with classical results of heat transfer on a flat plate. The method becomes fully predictive provided the roughness of the liquid vapour interface, which strongly influences heat transfer, is specified (Fruman *et al.* 1999).

Brennen (1994) introduces a thermodynamic parameter Σ defined by:

$$\Sigma = \frac{\rho_v^{\,2}\, L^2}{\rho_l^{\,2}\, c_{pl}\, T\, \sqrt{a}}$$

whose units are $m/s^{3/2}$ and proposes a criterion to determine if the cavitation process is thermally controlled or not. Kato (1984) introduces a very similar parameter, named α, which differs from Brennen's parameter only by the power of the ratio ρ_v/ρ_l which is 1.5 instead of 2.

The present contribution is limited to an experimental analysis of the effect of temperature on the development of leading edge cavitation on a four-bladed inducer working with a refrigerant. The basis of the approach is the classical assumption of similarity of cavity developments for equal cavitation parameters.

Two cavitation parameters are usually defined. One is based upon the vapor pressure estimated at the liquid temperature at infinity T_∞ :

$$\sigma = \frac{p_{ref} - p_v(T_\infty)}{\rho_l \, \omega^2 R^2} \tag{1}$$

and the other one on the actual pressure p_c inside the cavity:

$$\sigma = \frac{p_{ref} - p_c}{\rho_l \, \omega^2 R^2} \tag{2}$$

Both parameters are related by:

$$\sigma = \sigma_c - \frac{p_v(T_\infty) - p_c}{\rho_l \, \omega^2 R^2} \tag{3}$$

The pressure inside the cavity is generally considered as the sum of the vapor pressure of the tested liquid and the partial pressure of dissolved gases, if any:

$$p_c = p_v(T_c) + p_{gases} \tag{4}$$

In Equation (4), the vapor pressure is estimated at the actual temperature inside the cavity T_c , which is lower than the temperature at infinity T_∞ because of the thermal effect. The pressure difference:

$$\Delta p_v = p_v(T_\infty) - p_v(T_c) \tag{5}$$

is a measure of the thermodynamic effect. By combining equations (3) to (5), we obtain:

$$\sigma = \sigma_c - \frac{\Delta p_v}{\rho_l \, \omega^2 R^2} + \frac{p_{gases}}{\rho_l \, \omega^2 R^2} \tag{6}$$

The second term accounts for the increase of pump performance due to thermal effects whereas the third one accounts for its decrease because of dissolved gases.

Although dissolved gases may have a non negligible influence, their contribution will be ignored in the present study because of the lack of information on the values of the coefficients of diffusion and of their variations with the temperature, especially in the present case of diffusion of air in refrigerant 114. Because of the high capability of refrigerants to dissolve air, the question of dissolved gas content could be a serious limitation of this work.

In the absence of any dissolved gas effect, Equation 6 reduces to:

$$\sigma = \sigma_c - \frac{\Delta p_v}{\rho_l \, \omega^2 R^2} \tag{7}$$

Let us compare a test N°1 with a significant thermal effect with a similar test N°2 without any thermal effect (in cold water for instance) and let us suppose that the σ values are adjusted so that the cavity lengths are equal for both tests. The equality of the σ_c values assumed here leads to:

$$\sigma_2 - \sigma_1 = \frac{\Delta p_v}{\rho_l \, \omega^2 R^2} \tag{8}$$

Hence, the thermodynamic effect Δp_v on test N°1 can be estimated from the measured difference in cavitation parameters $\Delta \sigma = \sigma_2 - \sigma_1$ between tests N°2 and N°1, provided the σ-values are adjusted to get similar developments of cavitation. This is the principle of the present study.

2. Experimental setup

The tests were carried out with refrigerant R114, whose thermodynamic properties lead to a significant thermal effect at the ambient temperature. The liquid temperature in the testing facility could be changed between 20°C and 40°C. The pressure was also controlled, together with the flowrate and the rotation speed of the machine. Figure 1 presents a schematic view of the facility.

The tests consisted in visualizations of leading edge cavitation for various operating conditions. A photograph is taken for each blade. The cavity length is measured on each photograph and the mean value is calculated. This procedure is used to get rid of a possible scattering in the case of non-balanced cavitation.

The cavity length is measured along a unique radius, which corresponds to a mean position between hub and casing. The cavity length along this mean radius appeared to be a good estimate of the extent of the leading edge cavity and in particular not too much influenced by tip-leakage cavitation. Three-dimensional effects were not considered in the present work.

To measure the cavity length, a grid was drawn directly on the inducer blades (Figure 2). A reference photograph of the grid was taken and superimposed to all the photographs. Such a procedure was used to minimize the distortions due to the windows. The cavity length is measured by the angle from the leading edge. The origin 0 deg corresponds to the position of the leading edge.
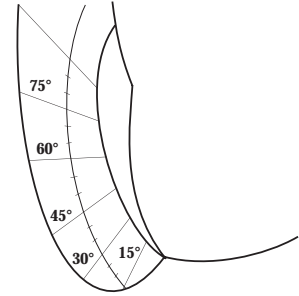
Fig.2: The grid used for cavity length measurement

In addition, pressure fluctuations were measured by means of pressure transducers, flush mounted on the casing. Among the various transducers, we choose to consider the one which is located at the level of the blade leading edges. Former studies have shown that this location is the most suitable to identify cavitation instabilities. The various regimes are recognized from a spectral analysis of the pressure fluctuations. They were also observed under stroboscopic lighting.
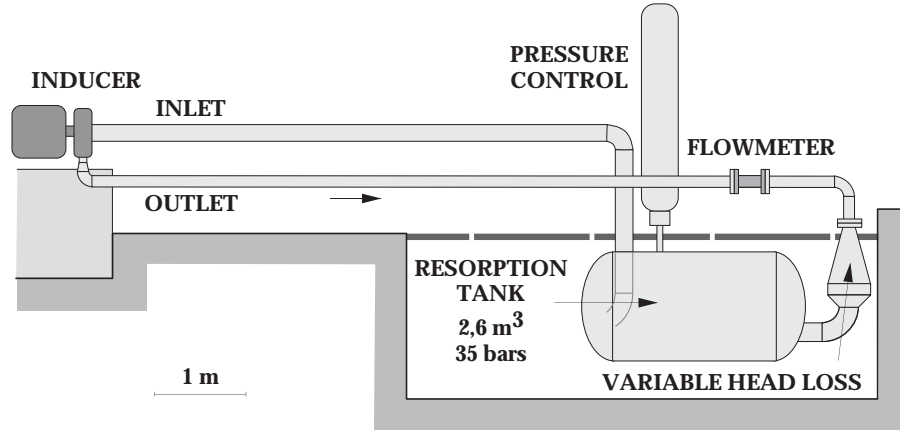
Figure 1 : Schematic view of the facility

3. Visualizations

Figure 3 presents typical visualizations of the leading edge cavity at nominal flowrate, constant temperature (20°C) and constant speed of rotation (5500 rpm). These photographs were taken during a cavitation test and are relative to decreasing values of the cavitation parameter. They all correspond to the same blade. It has to be noted that different types of instabilities occur during the cavitation test (see section 5). Hence, the observation of a unique blade is not sufficient to have an accurate information on the general development of the cavitation. At the end of the test ($\sigma = 0.0058$), bubbles are visible at the inlet. They are probably due to the degassing of the liquid which proved to be strongly aerated.

We can observe that the closure line of the cavity is reasonably well defined in the central part of the blade, where the measurements are done. It can also be observed that the detachment of the leading edge cavity, in the neighborhood of the hub, occurs somewhat upstream of its position on the rest of the blade. It is due to the shape of the leading edge which is slightly beveled. As a consequence, the cavity appears slightly longer at hub.

Figure 4 presents visualizations of the leading edge cavity at a constant cavitation number, for three different temperatures 20°C, 30°C and 40°C. The flowrate, as well as the speed of rotation are kept constant. This figure clearly shows that the cavity shrinks with increasing temperature, as expected because of the increase of thermal effects with the temperature. This trend will be quantified in section 5.
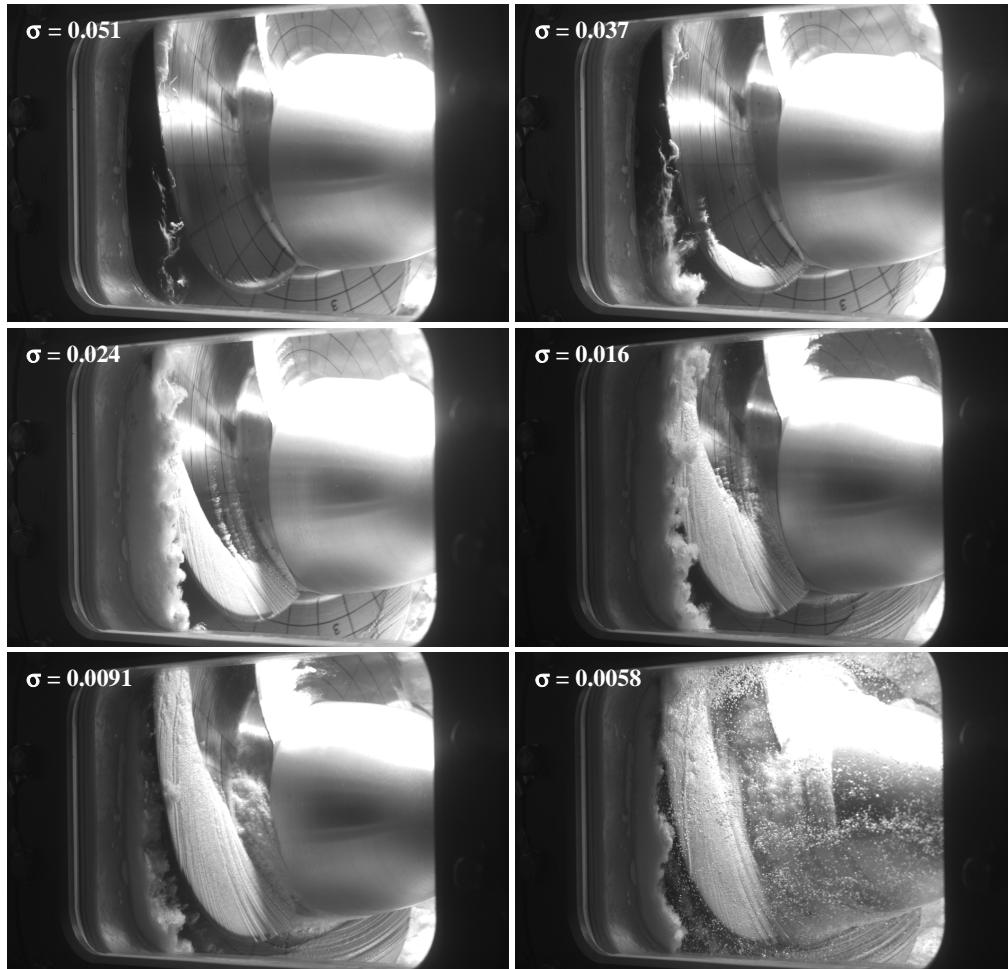
Figure 3: Visualization of the leading edge cavity on the four-bladed inducer working with refrigerant R114 for different values of the cavitation parameter (Rotation speed: 5500 rpm, nominal flowrate, liquid temperature: 20°C, blade #4)
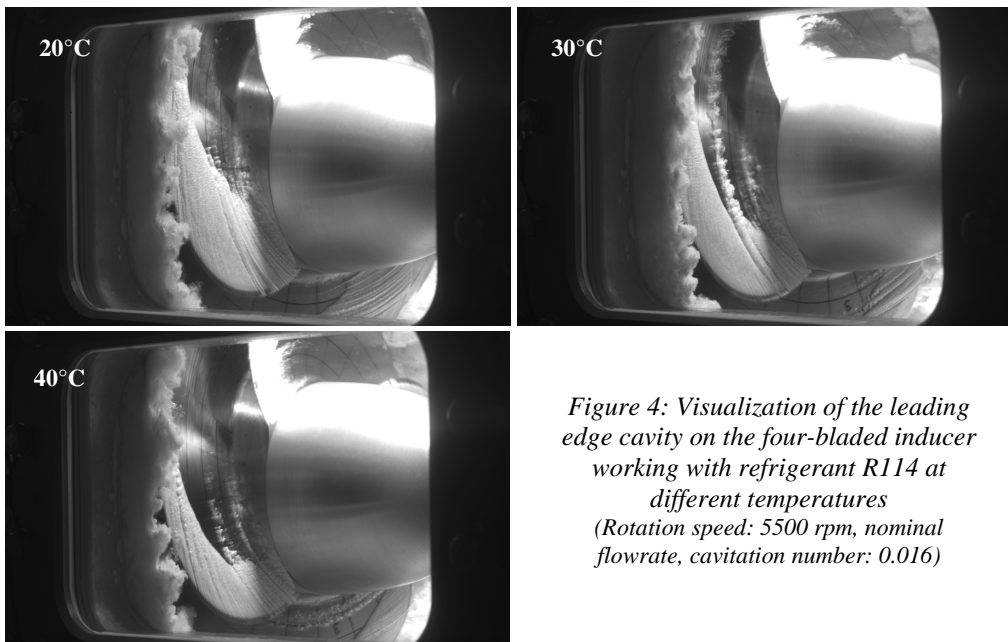

Figure 4: Visualization of the leading edge cavity on the four-bladed inducer working with refrigerant R114 at different temperatures (Rotation speed: 5500 rpm, nominal flowrate, cavitation number: 0.016)

4. Pressure spectra and cavitation instabilities

Figure 5 presents two spectral maps obtained at two different temperatures, 20°C and 40°C. The color represents the amplitude of the spectra. For both tests, the speed of rotation is 5500 rpm and the corresponding frequency is f = 91.7 Hz. The blade passage frequency 4f is easily identified.

During the cavitation test, as the cavitation parameter is gradually decreased, we first observe the occurrence of the component 2f which is the signature of alternate blade cavitation. The visualizations confirm the existence of two small and two longer cavities.
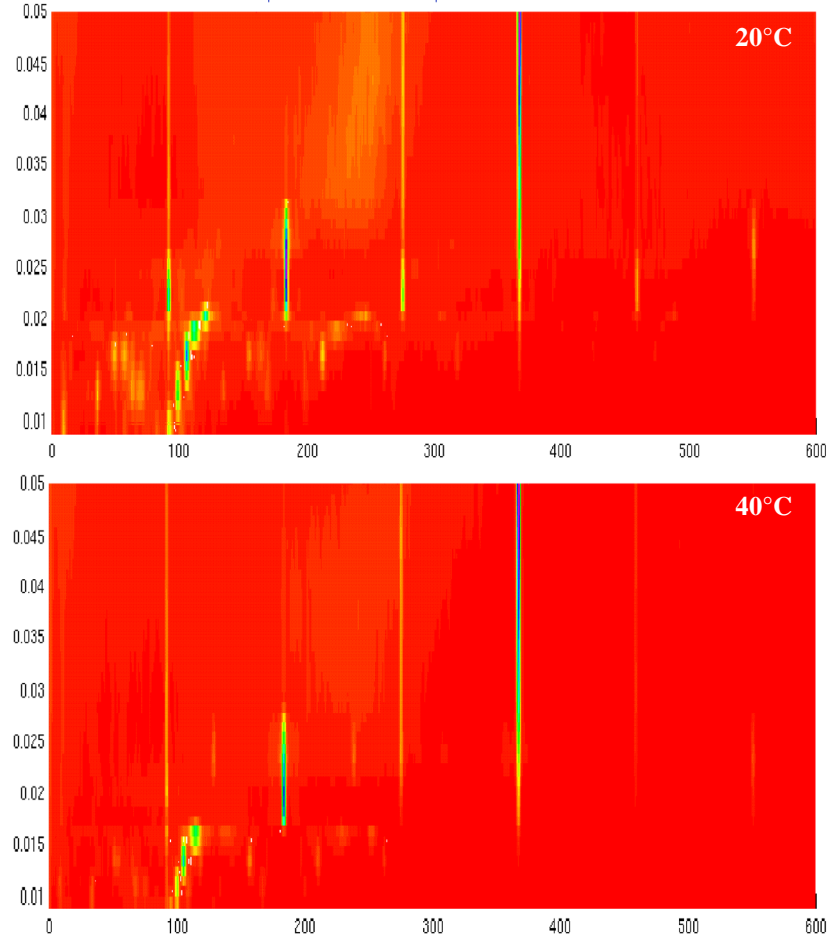

*Figure 5: Maps of pressure fluctuation spectra in refrigerant R114 at two different temperatures
20°C and 40°C (rotation speed 5500 rpm, nominal flow rate). The abscissa is the frequency
in Hz and the ordinate the cavitation parameter. The color represents the amplitude of the spectra.*

A further decrease in cavitation parameter leads to the extinction of alternate blade cavitation and the onset of rotating cavitation with a component slightly higher than the rotation frequency f. These regimes were already identified by several experimenters (see e.g. Goirand *et al.* 1992, Tsujimoto 2001).

As the cavitation parameter is decreased, the characteristic frequency of rotating cavitation is progressively shifted towards the rotation frequency and is finally tuned to it. For smaller values of the cavitation parameter, no cavitation instabilities are observed and the four cavities are equally developed on each blade.

The two maps obtained at two different temperatures are qualitatively similar and the same regimes are identified. The differences principally lie in the thresholds. The onset of alternate blade cavitation as well as rotating cavitation are delayed as the temperature is increased. This trend is consistent with the thermodynamic effect which is known to cause a delay in the development of cavitation. It will be quantified in section 6.

5. Cavity lengths

A systematic analysis of the photographs allowed us to plot the evolution of the cavity length ℓ with the cavitation parameter σ (Figure 6). The various regimes of instability deduced from the analysis of the pressure fluctuations spectra are also indicated. The data are all relative to decreasing cavitation parameter. Hysteresis effects were not considered.

For each value of the cavitation parameter, four points are shown, which correspond to each blade. The mean value is also plotted together with the RMS value. At high cavitation number, before the onset of any cavitation instability, the four cavities have almost the same length. The scattering increases with the onset of instabilities, as expected.
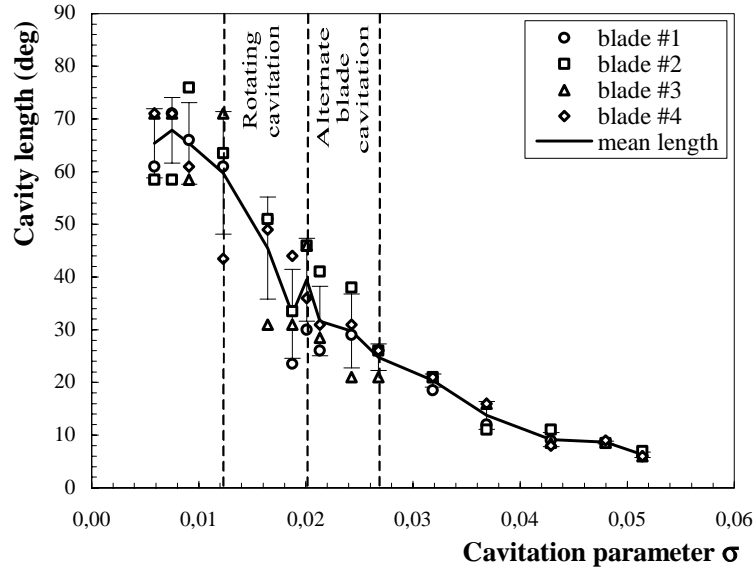

Figure 6: Cavity length vs cavitation number at nominal flow rate, 5500 rpm and 20°C. (The cavity length is measured by the angle from the leading edge. The first point on the right-hand side corresponds to cavitation inception; the cavity length is not exactly zero because of the beveled edge. The last point on the left-hand side corresponds to a two-phase flow at the pump inlet)
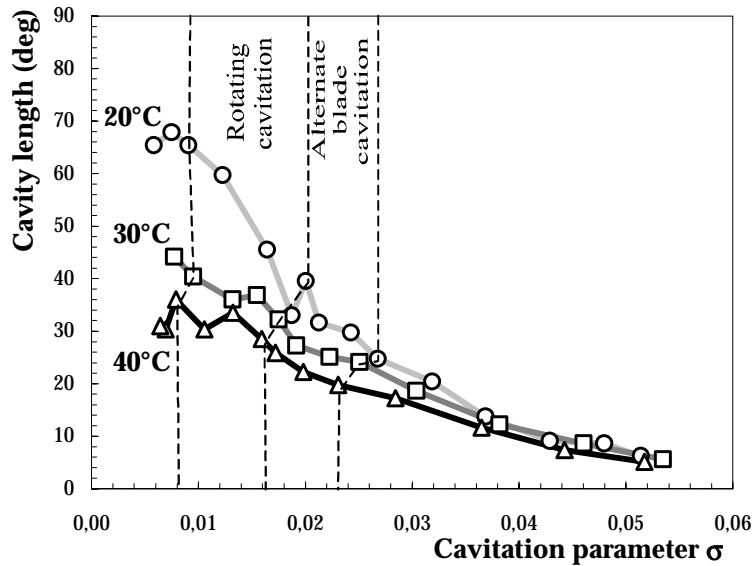

Figure 7: Influence of the temperature on the evolution of the cavity length with the cavitation number and on the onset of cavitation instabilities for the four-bladed inducer working with refrigerant R114 (Rotation speed : 5500 rpm, nominal flowrate). The plotted cavity lengths are mean values for the four blades.

A similar analysis is done for two other temperatures 30°C and 40°C and the results are compared on Figure 7. The trend which was observed on the photographs of Figure 4 for a given value of the cavitation parameter is confirmed here for the whole curves $\ell(\sigma)$: the higher the temperature, the shorter the cavity.

The onset of the two regimes of instability observed, i.e. alternate blade cavitation and rotating cavitation, are also indicated on Figure 7. The threshold values were determined during the cavitation tests by detecting the appearance of the corresponding component on the spectra.

Using these curves, the thermodynamic effect can be estimated on the basis of the approach presented in the introduction. For a given cavity length, i.e. along a horizontal line in Figure 7, the difference in the values of the cavitation parameter can be considered as an indirect measure of the thermodynamic effect.

6. Concluding remarks on the thermodynamic effect

The thermodynamic effect appears negligible for small enough cavities and increases gradually with the development of cavitation. The table below gives the order of magnitude of the thermodynamic effect which was estimated from Figure 7 for two different cavity lengths and two different temperatures 30°C and 40°C.

Table 1: Estimates of the thermodynamic effect on the basis of cavity length

	20→30°C	30°C			20→40°C	40°C		
Cavity length	$\Delta\sigma$	Δp (bars)	ΔT (°C)	**B-factor**	$\Delta\sigma$	Δp (bars)	ΔT (°C)	**B-factor**
20 deg	.0032	.13	1.7	**1.1**	.0071	.28	2.9	**1.4**
35 deg	.0061	.24	3.1	**2.0**	.0136	.54	5.6	**2.8**

The estimation of the thermodynamic effect requires reference results without thermal effects, in cold water for instance, as explained in section 1. Because of differences in experimental procedures and operating conditions between tests in water and R114, it was chosen to consider the present results at the lowest temperature 20°C as the reference ones, in a first approach. As we know that the thermal effects are actually not fully negligible at 20°C in refrigerant 114, the so-estimated thermodynamic effect can be considered as undervalued.

In table 1, the quantity $\Delta\sigma$ represents the shift in cavitation parameter which ensures similar cavitation extents at two different temperatures. Δp is the thermodynamic effect in terms of vapor pressure difference, whereas ΔT is the thermodynamic effect in terms of temperature difference. Also indicated is the classical B-factor. The energy balance can be written as follows:

$$\rho_v \, \vartheta_v \, L = \rho_l \, \vartheta_l \, c_{pl} \, \Delta T$$

where ϑ_l is the volume of liquid which provides the heat for the vaporization of the volume ϑ_v of vapor. Hence, the B-factor can be calculated by:

$$B = \frac{\vartheta_v}{\vartheta_l} = \frac{\Delta T}{\Delta T^*}$$

The present estimation of the thermodynamic effect lies upon the curves $\ell(\sigma)$. Another criterion based upon the regimes of instability can be used. In table 2, we indicate the shifts in cavitation number observed for the onset of alternate blade cavitation and rotating cavitation, together with the corresponding pressure and temperature differences.

In comparing the results of Tables 1 and 2, it appears that the second criterion based on cavitation instabilities leads to estimates of the thermal effects significantly smaller than the first one based on cavity lengths, whereas we should have expected the instabilities to occur for similar developments of cavitation. This phenomenon is also clear from Figure 7 where it can be seen that the inception of alternate blade cavitation as well as rotating cavitation do not occur for a constant length of the leading edge cavity. Several difficulties listed below can be suspected.

First of all, the onset of cavitation instabilities were determined during the cavitation test from the visual appearance of the corresponding component in the spectra. A more objective procedure is needed.

In the present study, only the leading edge cavity is considered, but other types of cavitation and particularly tip-leakage cavitation could play a role in the onset of cavitation instabilities. It might be important to quantify not only the volume of the leading edge cavity but the total volume of cavitation including tip-leakage cavitation.

We can also suspect a difficulty concerning the basic assumption according to which the cavities have the same extent for equal σ_c values, as already questioned in former experiments conducted with the same liquid on a venturi (Belahadji *et al.* 1997). This scaling law lies on the classical model of a cavity of pure vapor and constant pressure, although measurements of void fraction inside the cavity tend to prove that it is rather made of a two-phase mixture with a mean void fraction significantly lower than 1 (Fruman *et al.* 1999).

Finally, we should mention that the present tests were conducted with a liquid strongly aerated and we do not know yet quantitatively the influence of dissolved gas content. This work is in progress to try to clear up these still open questions and develop a procedure for the prediction of the thermodynamic effect.

Table 2: Estimates of the thermodynamic effect on the basis of the onset of instabilities

	20→30°C	30°C			20→40°C	40°C		
Regime of instability	Δσ	Δp (bars)	ΔT (°C)	**B-factor**	Δσ	Δp (bars)	ΔT (°C)	**B-factor**
Alternate blade cavitation	.0017	.068	.88	**.56**	.0026	.10	1.1	**.51**
Rotating cavitation	.0037	.15	1.9	**1.2**	.0042	.16	1.7	**.83**

References

Belahadji B. Franc J.P. & Michel J.M. 1997 "Analyse des effets thermiques en cavitation à partir d'essais au forane" La Houille Blanche 4/5 117-122 (in french)

Billet M.L. 1970 "Thermodynamic effects on developed cavitation in water and Freon 113 *PhD thesis*

Billet M.L. Holl J.W. & Weir D.S. 1981 "Correlation of thermodynamic effects for developed cavitation" *J. of Fluids Eng.* **103** 534-542

Bonnin J. 1973 "Theoretical and experimental investigations of incipient cavitation in different liquids *J. of Basic Eng.* 1-8

Brennen C.E. 1994 "Hydrodynamics of pumps" Concept ETI, Inc. and Oxford University Press

Delannoy Y. & Reboud J.L. 1993 "Heat and Mass Transfer on a Vapor Cavity" *Gas-Liquid Flows Symposium* Washington ASME-FED **165** June 1993

Fruman D.H. Benmansour I. & Sery R. 1991 "Estimation of the thermal effects on cavitation of cryogenic liquids" FED-Vol.109 *Cavitation and Multiphase Flow Forum* ed. O. Furuya & H. Kato Portland June 23-27 93-100

Fruman DH. Reboud JL. & Stutz B. 1999 "Estimation of the Thermal Effects in Cavitation of Thermosensible Liquids" *Int. J. Heat and Mass Transfer* **42** 3195-3204

Goirand B. Mertz A.L. Joussellin F. & Rebattet C. 1992 "Experimental investigations of radial loads induced by partial cavitation with a liquid hydrogen inducer" *3rd Int. Conf. On Cavitation ImechE* Cambridge UK **C453/056** 263-269

Holl J.W. Billet M.L. & Weir D.S. 1975 "Thermodynamic effects on developed cavitation" *J. of Fluids Eng.* 507-514

Hord J. 1972a 1972b 1973 1974 "Cavitation in liquid cryogens" Vol. I II III & IV NASA CR-2054/2156/2242/2448

Kato H. 1984 "Thermodynamic effect on incipient and developed sheet cavitation" *Proc. Int. Symp. On Cavitation Inception New-Orleans* Dec.9-14 ed. B.R. Parkin & W.B. Morgan FED **Vol.16** 127-136

Kovich G. 1970 "Comparison of predicted and experimental cavitation performance of 84° helical inducer in water and hydrogen" NASA TN D-7016

Moore R.D. & Ruggeri R.S. 1968 "Prediction of thermodynamic effects of developed cavitation based on liquid-hydrogen and freon-114 data in scaled venturis" NASA TN D-4899

Reboud J.L. Sauvage E. & Desclaux J. 1990 "Partial Cavitation Model for Cryogenic Fluids" *Cavitation & Multiphase Flow Forum*, Toronto, ASME-FED **vol. 98**, June 1990

Ruggeri R.S. & Moore R.D. 1969 "Method for prediction of pump cavitation performance for various liquids, liquid temperatures and rotative speeds" NASA TN D-5292

Stepanoff A.J. 1964 "Cavitation properties of liquids" *J. of Eng. for Power* April 1964 195-199

Tsujimoto Y. 2001 "Simple rules for cavitation instabilities in turbomachinery" *Proc. 4th Int. Symp. on Cavitation* Pasadena June 20-23